Observation of Fast Current Redistribution in an Imploding Plasma Column

C. Stollberg,[1,*] E. Kroupp,[1] D. Mikitchuk,[1] P. Sharma,[1] V. Bernshtam,[1] M. Cvejić,[1] R. Doron,[1] E. Stambulchik,[1] Y. Maron,[1] A. Fruchtman,[2] I. E. Ochs,[3] N. J. Fisch,[3] and U. Shumlak[4]

[1]*Weizmann Institute of Science, Herzl Street 243, 7610001 Rehovot, Israel*
[2]*Department of Physics, Holon Institute of Technology, Holon 58102, Israel*
[3]*Department of Astrophysical Sciences, Princeton University, Princeton, New Jersey 08540, USA*
[4]*Aerospace and Energetics Research Program, University of Washington, Seattle, Washington 98195, USA*

(Received 9 November 2021; revised 10 March 2023; accepted 3 May 2023; published 19 May 2023)

Spectroscopic measurements of the magnetic field evolution in a Z-pinch throughout stagnation and with particularly high spatial resolution reveal a sudden current redistribution from the stagnating plasma (SP) to a low-density plasma (LDP) at larger radii, while the SP continues to implode. Based on the plasma parameters it is shown that the current is transferred to an increasing-conductance LDP outside the stagnation, a process likely to be induced by the large impedance of the SP. Since an LDP often exists around imploding plasmas and in various pulsed-power systems, such a fast current redistribution may dramatically affect the behavior and achievable parameters in these systems.

DOI: 10.1103/PhysRevLett.130.205101

Introduction.—The force exerted on a plasma by a current and its associated magnetic field governs various processes in space and laboratory plasmas [1–16]. The implosion of a current-carrying plasma column, as in Z-pinches, is a typical example where the current distribution in the plasma plays a crucial role [5–7]. In this configuration, the plasma is generated by a pulsed current driven axially in a cylindrical gas or a metallic load. The current generates an azimuthal magnetic field B_θ that accelerates the plasma radially inward and implodes together with the plasma [5–10]. Thus, a Z-pinch is a platform for investigating the interplay between the current density distribution and the evolution of the implosion and stagnation, which is highly complex [5–7,10,17–19].

A detailed analysis of the energy and pressure balance of two Z-pinch plasmas, distinctly different in power [20], revealed that, in both the low- and high-power systems, the magnetic pressure due to B_θ is small at the stagnating plasma (SP). Contrary to what had been believed, at most $1/3$ of the discharge current was found to flow within the SP. The direct confirmation of this result required experimental measurements of B_θ during the stagnation and close to the SP, a task that is challenging due to the high electron density n_e, the high ion velocities, and the transient nature of the plasma [21].

A few studies reported on the direct measurement of magnetic fields in Z-pinches [22–29]. Those performed at large radii during the early stage of implosion [22–25] demonstrate that in general the discharge current flows in the imploding plasma. Also, studies performed at the time of stagnation [26–28], outside the SP but close enough to it, confirmed that only a small fraction of the current flows in the compressed SP, while the majority of the current flows at larger radii. In this Letter, we address the mechanism that leads to the low current at stagnation by measuring the temporal evolution of the current density radial distribution throughout the entire implosion and stagnation, down to the small radius of the SP, in particular with a high spatial resolution.

The measurements revealed that in the section close to the cathode (1) the entire current flows in the imploding plasma until stagnation, (2) the current then suddenly redistributes from the small radius of the stagnation to larger radii where a hollow low-density plasma (LDP) resides, and (3) while the current transitions to larger radii, the SP continues to implode.

This detailed observation of the fast current redistribution was obtained from temporally and radially resolved measurements of the local magnetic field in a small-scale gas-puff Z-pinch, where the initial gas distribution was peaked on axis, thus allowing for satisfactory reproducibility and symmetry by mitigating the Magneto-Rayleigh-Taylor instabilities [30,31]. The diagnostics, based on Zeeman-polarization spectroscopy, allowed for determining B_θ, even when the Zeeman-split pattern was obscured by the line broadening [22,24,26,27,32]. Also, the radial distribution of charge states in the plasma was used as in [22,26,27] to obtain B_θ locally as a function of r, from chordal measurements, without the need to inverse Abel transform the observed line shapes (no azimuthal uniformity is assumed) [26,27]. Also, the measurements of the plasma parameters allowed for inferring the plasma resistivity required for the interpretation of the present results.

Our findings are likely related to the previous observations of low current in the SP of Z-pinches [10,20,26–28] and the phenomenon of "trailing" current [10,24–27,33–38],

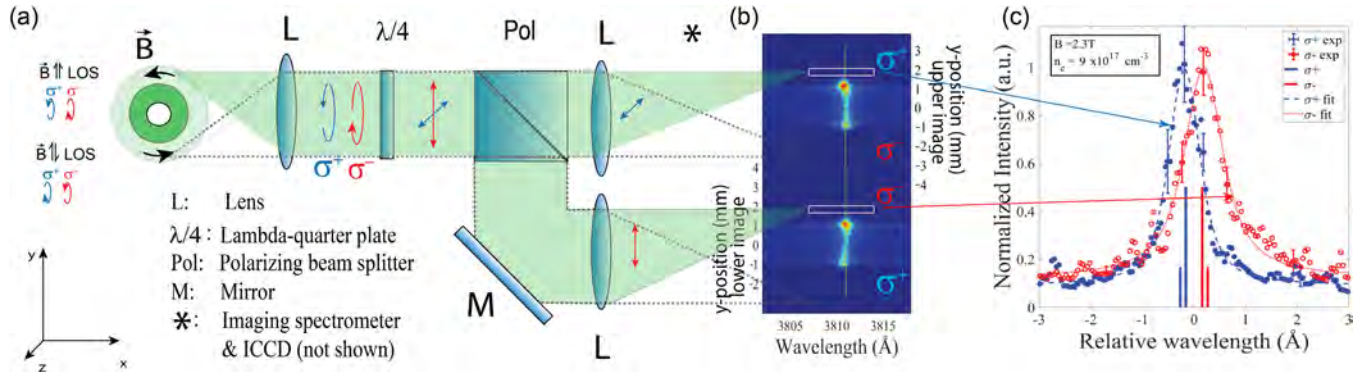

FIG. 1. Schematics for B-field determination. (a) Diagnostic setup: with the side-on imaging, at the outermost chord, the LOS is parallel to $\vec{B}$ so that only the circularly polarized σ^+ and σ^- Zeeman components are observed. The light is transformed into orthogonal, linearly polarized light by a $\lambda/4$ plate and spatially separated by a polarizing beam splitter. The two plasma images, with the different polarization properties, are defracted by a 1-m imaging spectrometer and recorded on an intensified charge-coupled device (not shown on the image). (b) Typical spectral recording of the O VI 3s–3p transition obtained at $t = 100$ ns. The green line represents the unshifted spectral line, illustrating the deviation of the measured spectral lines from the unperturbed position, where σ^+ and σ^- exhibit blue and red (B-dependent) shifts, respectively. (c) Spectral lineouts (markers) taken from (b) at $y = 1.6 \pm 0.1$ mm from the upper and the lower image (bright rectangles) and their fit (dashed/dotted). The solid lines represent the calculated Zeeman pattern without line broadening. The separation between the profiles of 0.37 Å yields a B-field of 2.3 T, and the Stark broadening yields $n_e \approx 9 \times 10^{17}$ cm^{-3} [40,41].

and might also be relevant for lower-density plasma systems [10], such as plasma switches [11–13] and high power transmission lines [14,15].

Experimental methods.—In the present experiment [39], an oxygen column of initial diameter ≈ 3 mm and mass of (1.6 ± 0.6) μg/cm is injected into a 6-mm-long anode-cathode gap and imploded by a current pulse rising to 27 kA in 160 ns.

For determining the B-field, the wavelength separation between the σ^+ and the σ^- Zeeman components is measured [21]. Employing a side-on imaging (Fig. 1) the line of sight (LOS) through the outermost chord of a spectral line emission is parallel to B_θ, which allows for spatially separating the σ Zeeman components and recording them simultaneously on a single detector coupled to an imaging spectrometer. The spectroscopic system spectral, temporal, and spatial resolutions are 0.3 Å, 10 ns, and 100 μm ($\approx 1/5$ of the SP radius), respectively. In order to obtain B_θ at different radii, we use up to three different spectral lines that are radially separated [26].

A second imaging spectroscopic setup, providing a broader spectrum [39], is used for temperature (from line intensity ratios [42–44]) and density (from Stark broadening [40,41,45] and absolute intensity [43]) diagnostics, as well as the estimation of the average charge state Z_{eff}, which yields the plasma resistivity.

Results.—Presented are results obtained at $z = 1$ mm from the cathode valve. Figure 1(b) shows a typical spectral recording of the chord-integrated plasma emission, split into two images with different polarizations, as described above. To determine the B-field, spectral lineouts [Fig. 1(c)] are extracted at the outer edge of the O VI spectral line and fitted with Voigt profiles. The fitting accounts for the Zeeman components (0.1 Å), the Gaussian contributions from the instrumental and Doppler broadenings (0.4 Å) and the Lorentzian contribution (0.6 Å) from the Stark broadening. For the 3s–3p transition of O VI at 3811.35 Å, the separation of the Zeeman σ components is 0.16 Å for $B = 1$ T [21]. For the example in Fig. 1(c) we find $B_\theta = 2.3^{+0.4}_{-0.2}$ T, where the uncertainty includes the fitting error, spectrometer aberrations, and the performance of the polarization optics [26,39]. The Stark broadening allows for determining the electron density $(0.9 \pm 0.3) \times 10^{18}$ cm^{-3} [40,41]. The integration region in the radial direction is defined for each spectral lineout individually, depending on signal-to-noise ratio and line broadening, and is typically 100 to 200 μm.

Figure 2 summarizes the results of the B-field measurements at different times during the implosion ($t < 140$ ns) and at stagnation ($t = 140$ to 170 ns), demonstrating the fast current redistribution. For any given time, we used the charge state that resides at the outermost radius of the imploding plasma. Its emission-intensity radial distribution is shown along with the B_θ values obtained at the outer edge r_{out} of its line emission. Also shown is B_θ obtained by assuming that the entire current $I(t)$, measured by a calibrated B-dot probe [90% of $I(t)$ is considered as the entire current], flows within the radius of the B-field measurement, namely $B_{\text{B-dot}}(t) = 0.9\mu_0 I(t)/2\pi r_{\text{out}}(t)$. We note that each data point was obtained in a separate discharge, with shot-to-shot variations significantly smaller than the error bars quoted in Fig. 2. For $t \leq 140$ ns, the data show a good agreement between the measured (Zeeman) and the expected (B-dot) B-field values, indicating that the entire discharge current flows in the imploding plasma. At

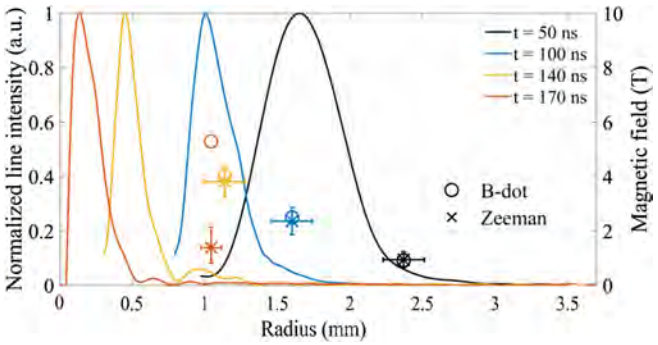

FIG. 2. Evolution of the O IV ($t = 50$ ns) and O VI ($t \geq 100$ ns) emission intensity radial distribution along with the magnetic field measured at the outer chord: at $t = 50$–140 ns, the agreement between expected (B-dot) and measured magnetic field (Zeeman) indicates the confinement of the entire discharge current in the imploding plasma. At $t = 170$ ns the fraction of the current that can be located in the stagnating plasma is $\lesssim 30\%$.

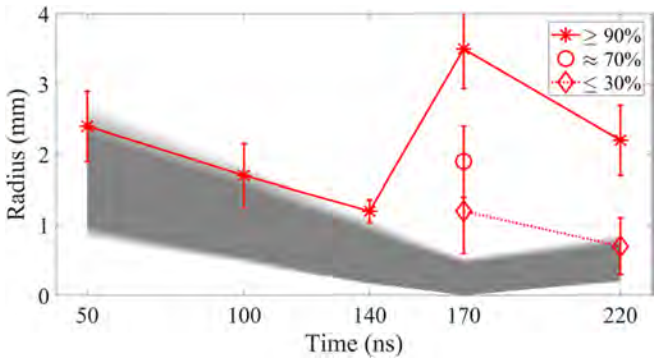

FIG. 3. Gray: location of the plasma with $n_e > 0.1 n_{e,\max}$ (from continuum radiation intensity) with uncertainty in light gray. Red: locations at which a certain percentage of the discharge current was measured. At $t \geq 170$ ns the measurements were obtained in an LDP with a density lower than 10% of $n_{e,\max}$. Initially, the current implodes together with the main plasma, while at stagnation (140–170 ns), a sudden current redistribution to much larger radii takes place.

$t = 170$ ns, however, a significant discrepancy is observed: at most, 30% of the discharge current flows within the stagnating plasma that is located at $r < 1.1$ mm.

At the time of stagnation, we also use additional transitions from the LDP to obtain the current density distribution at $r > 1.1$ mm. The O IV 3p–3d transition at 3736.85 Å is used to obtain a B-field of 1.7 T at $r = 1.9 \pm 0.35$ mm, corresponding to 70% of the discharge current. The O III 3s–3p transition at 3759.87 Å, residing at $r > 2.3$ mm, yields a B-field of ≥ 1.3 T at $r = 3.55 \pm 0.21$ mm, corresponding to the entire discharge current.

To demonstrate the correlation between the current evolution and the plasma implosion, we plot in Fig. 3 the position of the imploding plasma (gray area) along with the positions at which the entire discharge current was measured (red line). Additionally, for $t \geq 170$ ns, we show the positions that enclose $\approx 70\%$ and $\leq 30\%$ of the discharge current. It is seen that during the implosion ($t < 140$ ns), the current implodes together with the main plasma, while at stagnation ($t = 140$ to 170 ns) a current redistribution occurs to an LDP at larger radii. This demonstrates a nonmonotonic evolution of the current channel, which is initially shrinking in radius, followed by a fast expansion. Remarkably, the stagnating plasma continues its inward motion as the current moves outward and remains outside the SP for several tens of nanoseconds. Subsequently, the SP expands due to thermal pressure while an inward motion of the LDP is observed.

Discussion.—It was shown that the entire driven current is carried by the imploding plasma until the stagnation before a rapid transfer of the current from the SP to a LDP region at the plasma periphery occurs, revealing a transition that has not been observed as yet.

We now turn to examine possible mechanisms for the current transfer. Recently, it was shown that in a zero-resistivity plasma, the current channel is expected to move radially outward when the imploding plasma velocity profile $v_r(r)$ satisfies $\partial(|v_r|/r)/\partial r < 0$ [46]. This condition is satisfied up to stagnation at 170 ns, as the LDP hardly moves. To explain the rapid current redistribution that begins only after 140 ns, resistive effects must be considered. Indeed, we find that it is the rapid resistance change in the LDP that can explain the observed fast current redistribution.

We assume that, initially, the LDP is a weakly ionized gas (left behind from the initial gas distribution) with a resistivity much larger than that of the SP. An electric field is induced in the LDP due to the SP implosion that increases T_e and leads to a fast ionization and drop of the LDP resistance below the SP impedance.

To model the process of the partitioning of the discharge current $I = I_1 + I_2$ between I_1, the current through the SP, and I_2, the current through the LDP, we use a lumped-circuit equation (LCE): $d(LI_1)/dt = -I_1 R_1 + I_2 R_2$, representing the circuit illustrated in Fig. 4, where R_1 and R_2 are the resistances of the SP and the LDP, respectively, along $l = 2$ mm near the cathode. We write the inductance as $L = (\mu_0 l/2\pi) \ln(r_2/r_1)$, where r_1 and r_2 are the radii of the SP and of the LDP (the LDP is assumed to be relatively thin, as will be supported by experimental data elsewhere).

To illustrate the current partitioning I_2/I, the LCE can also be written as $L dI_2/dt = -(Z_1 + R_2)I_2 + Z_1 I$, where $Z_1 = R_1 + dL/dt$ is the SP impedance. Thus, the LCE captures the physics of both, the inductive current escape due to $dL/dt > 0$ during implosion [46], and the resistive model [47]. The LDP resistance is $R_2 = (m_e/e^2)(l/A)[(k_{eN} + \beta)N/n_e + k_{ei}]$, where A is the LDP cross section, $k_{eN}(T_e)$ and $k_{ei}(T_e)$ are the temperature dependent electron-neutral and electron-ion collision rate coefficients and $\beta(T_e)$ is the ionization rate

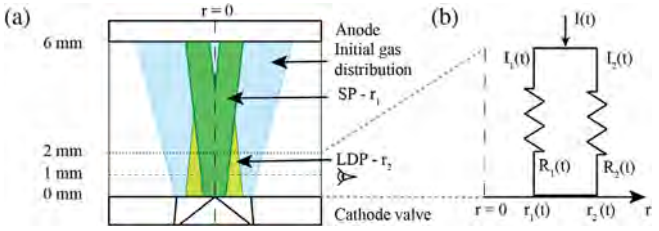

FIG. 4. (a) Schematic of the Z-pinch experiment with initial gas distribution, imploding and stagnating plasma (SP) and LDP featuring "zippering" effect. (b) Simplification of the 2-mm plasma element into a lumped-circuit model.

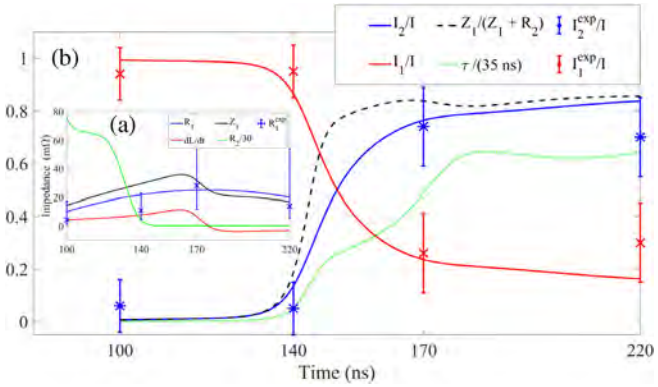

FIG. 5. Simulation of the lumped-circuit equation (LCE). (a) The abrupt decrease of the LDP resistance R_2 (green) enables the current transfer. (b) The evolution of the current partition I_2/I (blue) follows the impedance ratio (dashed black) with a delay of the current transfer time (dotted green).

coefficient [48], N is the density of atoms in the LDP, and m_e is the electron mass.

Using the measured $r_1(t)$ (Fig. 3), the approximately constant $r_2 = 2$ mm and $I = 20$ kA (for 100 ns < t < 220 ns) observed, and $R_1(t)$ as inferred from the measured SP parameters [39], we solve the equations for I_2 together with $dn_e/dt = \beta N n_e$. To determine $R_2(t)$, a linear rise in time of T_e from 0.5 eV at $t = 100$ ns to 12 eV at $t = 220$ ns was assumed for the LDP, consistent with the measured $T_e = (10 \pm 2)$ eV at $t = 170$ ns [39].

The simulated current evolution between 100–200 ns, shown in Fig. 5, occurs on three time scales: the SP implosion time, the ionization time of the LDP, and the current transfer time. The SP implodes under the magnetic pressure between 50 and 170 ns (see Fig. 3). This implosion time is about the Alfvén time $t_A \equiv r_0/v_A = (2r_0/I_1)\sqrt{\pi\lambda_1/\mu_0}$ (= 140 ns for $r_0 = 2.2$ mm, $I_1 = 20$ kA, and $\lambda_1 = 1.6 \times 10^{-7}$ kg/m). The implosion leads to an increase of R_1, dL/dt, and of Z_1 up to 35 mΩ at 165 ns [Fig. 5(a)]. Fast ionization of the LDP occurs around $t = 130$ ns. During the 20 ns ionization time, N/n decreases by 2–3 orders of magnitude. Subsequently, R_2 decreases from 2 Ω to ≈10 mΩ, below Z_1. This drastic decrease of the LDP resistance induces the current switching. The current transfer time is $\tau = L/(Z_1 + R_2)$. As long as R_2 is large, τ is short and I_2/I follows closely the impedance ratio $Z_1/(Z_1 + R_2)$. However, as R_2 becomes small, τ increases so that the current partitioning I_2/I lags behind the impedance ratio by ≈25 ns, consistent with the experimental observations. Note that τ is considerably shorter than the collisionless transfer time $L/(dL/dt)$, since the appropriate magnetic Reynolds number $(dL/dt)/R_1$ is smaller than unity.

We showed that in the presence of a LDP there arises a competition between the SP and the LDP for the discharge current. In the present experiment, the fast current redistribution can be explained by a drop of the LDP resistance R_2. Similarly, the current may transfer if Z_1 increases to $Z_1 > R_2$, due to a fast compression of the SP, or an increase of R_1, caused by a large resistivity or a small areal cross section [49]. Consistent with this picture, magnetohydrodynamics simulations performed in MACH2 [50] show that in a setup with a very high resistance R_2, resulting from the lack of ionization in MACH2, the entire discharge current flows in the SP throughout the stagnation. However, if the SP impedance Z_1 rises due to a forced compression of the SP to a (possibly unrealistic) small radius, a fast current transfer to a resistive LDP can be seen in the simulation.

Note that at locations farther away from the cathode, a gradually changing behavior is found: at $z = 3$ and 5 mm, the discharge current is never observed to flow at small radii [39], consistent with the absence of significant current in the stagnating plasma seen in previous gas-puff experiments [10,20,26,27]. A larger abundance of peripheral gas further away from the cathode due to a divergent initial gas distribution (see Fig. 4) results in an earlier diffusion of the current into the LDP forming a current that is *trailing* the imploding plasma. This trailing current, which flows continuously at radii much larger than the SP radius in regions with significant abundance of "trailing mass," has been observed previously [10,24–27] and was also indicated indirectly by imaging techniques and probe measurements [33–38].

Conclusions.—The fast current escape from the SP to much larger radii observed in the present work close to the cathode is most likely related to the previously reported phenomenon of low current at the stagnation of Z-pinches [10,20,26–28], trailing current [10,24–27,33–38], and possible "restriking" currents in wire-array Z-pinches [33,34,37]. These phenomena might be different manifestations of similar mechanisms, governed by the interplay of advection and diffusion, determined by the specific plasma and B-field parameters in these experiments. The fast current redistribution might also bear relevance to general pulsed-power systems, such as plasma switches [11–13] or transmission lines [14,15], where undesired plasmas of different sources, such as electrodes [14,15], instabilities [51,52], evaporation, and trailing mass in solid loads [33–38,53], boundary layers in gas loads [39], and unimploded plasma in Z-pinches [24],

may affect the system operation. Further investigations of the current switching should help with controlling it, achieving higher efficiency in current-pulse transmission, and producing higher energy-density plasmas [24]. Because of the fundamental aspects of this phenomenon it can also be relevant for investigations of space plasmas [54,55], and the evolution of the current distribution and energy balance in fusion plasmas [5,9,20].

The authors acknowledge enlightening discussions with A. Velikovich, V. Tangri, and Ya. E. Krasik, and are grateful to Brent Jones for valuable advice. U.S. gratefully acknowledges support of the Erna and Jakob Michael Visiting Professorship at the Weizmann Institute of Science. This work was supported in part by the Cornell Multi-University Center for High Energy Density Science (USA), by NSF-BSF (USA-Israel), by the DOE/NNSA via the Naval Research Laboratory (USA), by Sandia National Laboratories (USA), by the Israel Science Foundation, by the German Science Foundation (DFG TR18), by NNSA 83228-10966 [Prime No. DOE (NNSA) DE-NA0003764], and by NSF PHY-1805316.

*Corresponding author.
christine.stollberg@epfl.ch

[1] V. A. Rakov and M. A. Uman, *Lightning Physics and Effects* (Cambridge University Press, Cambridge, England, 2004), Vol. 59, p. 109.
[2] J. Chen, Physics of erupting solar flux ropes: Coronal mass ejections: Recent advances in theory and observation, Phys. Plasmas **24**, 090501 (2017).
[3] P. Tzeferacos *et al.*, Laboratory evidence of dynamo amplification of magnetic fields in a turbulent plasma, Nat. Commun. **9**, 591 (2018).
[4] M. Kikuchi, A review of fusion and tokamak research towards steady-state operation: A JAEA contribution, Energiespectrum **3**, 1741 (2010).
[5] D. B. Sinars, M. A. Sweeney *et al.*, Review of pulsed power-driven high energy density physics research on z at sandia, Phys. Plasmas **27**, 070501 (2020).
[6] D. D. Ryutov, M. S. Derzon, and M. K. Matzen, The physics of fast z pinches, Rev. Mod. Phys. **72**, 167 (2000).
[7] J. L. Giuliani and R. J. Commisso, A review of the gas-puff$z$-pinch as an x-ray and neutron source, IEEE Trans. Plasma Sci. **43**, 2385 (2015).
[8] S. A. Slutz and R. A. Vesey, High-Gain Magnetized Inertial Fusion, Phys. Rev. Lett. **108**, 025003 (2012).
[9] M. R. Gomez *et al.*, Experimental Demonstration of Fusion-Relevant Conditions in Magnetized Liner Inertial Fusion, Phys. Rev. Lett. **113**, 155003 (2014).
[10] Y. Maron, Experimental determination of the thermal, turbulent, and rotational ion motion and magnetic field profiles in imploding plasmas, Phys. Plasmas **27**, 060901 (2020).
[11] D. C. Black, R. J. Commisso, P. F. Ottinger, S. B. Swanekamp, and B. V. Weber, Experimental determination of gap scaling in a plasma opening switch, Phys. Plasmas **7**, 3790 (2000).
[12] J. T. Engelbrecht, N. D. Ouart, N. Qi, P. W. de Grouchy, T. A. Shelkovenko, S. A. Pikuz, J. T. Banasek, W. M. Potter, S. V. Rocco, D. A. Hammer, B. R. Kusse, and J. L. Giuliani, Enhancing the x-ray output of a single-wire explosion with a gas-puff based plasma opening switch, Phys. Plasmas **25**, 022704 (2018).
[13] B. V. Weber, R. J. Commisso, P. J. Goodrich, J. M. Grossmann, D. D. Hinshelwood, P. F. Ottinger, and S. B. Swanekamp, Plasma opening switch conduction scaling, Phys. Plasmas **2**, 3893 (1995).
[14] M. R. Gomez, R. M. Gilgenbach, M. E. Cuneo, C. A. Jennings, R. D. McBride, E. M. Waisman, B. T. Hutsel, W. A. Stygar, D. V. Rose, and Y. Maron, Experimental study of current loss and plasma formation in the z machine post-hole convolute, Phys. Rev. Accel. Beams **20**, 010401 (2017).
[15] N. Bennett, D. R. Welch, G. Laity, D. V. Rose, and M. E. Cuneo, Magnetized particle transport in multi-ma accelerators, Phys. Rev. Accel. Beams **24**, 060401 (2021).
[16] S. V. Lebedev, A. Frank, and D. D. Ryutov, Exploring astrophysics-relevant magnetohydrodynamics with pulsed-power laboratory facilities, Rev. Mod. Phys. **91**, 025002 (2019).
[17] D. Alumot, E. Kroupp, E. Stambulchik, A. Starobinets, I. Uschmann, and Y. Maron, Determination of the Ion Temperature in a High-Energy-Density Plasma Using the Stark Effect, Phys. Rev. Lett. **122**, 095001 (2019).
[18] E. Kroupp, E. Stambulchik, A. Starobinets, D. Osin, V. I. Fisher, D. Alumot, Y. Maron, S. Davidovits, N. J. Fisch, and A. Fruchtman, Turbulent stagnation in a z-pinch plasma, Phys. Rev. E **97**, 013202 (2018).
[19] S. Lebedev, D. Ampleford, S. Bland, S. Bott, J. Chittenden, C. Jennings, M. Haines, J. Palmer, and J. Rapley, Implosion dynamics of wire array z-pinches: Experiments at imperial college, Nucl. Fusion **44**, S215 (2004).
[20] Y. Maron, A. Starobinets, V. I. Fisher, E. Kroupp, D. Osin, A. Fisher, C. Deeney, C. A. Coverdale, P. D. Lepell, E. P. Yu, C. Jennings, M. E. Cuneo, M. C. Herrmann, J. L. Porter, T. A. Mehlhorn, and J. P. Apruzese, Pressure and Energy Balance of Stagnating Plasmas in z-Pinch Experiments: Implications to Current Flow at Stagnation, Phys. Rev. Lett. **111**, 035001 (2013).
[21] R. Doron, D. Mikitchuk, C. Stollberg, G. Rosenzweig, E. Stambulchik, E. Kroupp, Y. Maron, and D. Hammer, Determination of magnetic fields based on the zeeman effect in regimes inaccessible by zeeman-splitting spectroscopy, High Energy Density Phys. **10**, 56 (2014).
[22] G. Davara, L. Gregorian, E. Kroupp, and Y. Maron, Spectroscopic determination of the magnetic-field distribution in an imploding plasma, Phys. Plasmas **5**, 1068 (1998).
[23] M. R. Gomez, S. B. Hansen, K. J. Peterson, D. E. Bliss, A. L. Carlson, D. C. Lamppa, D. G. Schroen, and G. A. Rochau, Magnetic field measurements via visible spectroscopy on the z machine, Rev. Sci. Instrum. **85**, 11E609 (2014).
[24] D. Mikitchuk, M. Cvejić, R. Doron, E. Kroupp, C. Stollberg, Y. Maron, A. L. Velikovich, N. D. Ouart, J. L. Giuliani, T. A. Mehlhorn, E. P. Yu, and A. Fruchtman, Effects of a Preembedded Axial Magnetic Field on the Current Distribution in a z-Pinch Implosion, Phys. Rev. Lett. **122**, 045001 (2019).

[25] N. A. Aybar, F. Conti, M. Cvejic, D. Mikitchuk, M. Dozieres, E. Kroupp, J. Narkis, Y. Maron, and F. N. Beg, Dependence of plasma-current coupling on current rise time in gas-puff z-pinches, IEEE Trans. Plasma Sci. **50**, 2541 (2022).
[26] G. Rosenzweig, E. Kroupp, A. Fisher, and Y. Maron, Measurements of the spatial magnetic field distribution in a z-pinch plasma throughout the stagnation process, J. Instrum. **12**, P09004 (2017).
[27] G. Rosenzweig, E. Kroupp, T. Queller, A. Starobinets, Y. Maron, V. Tangri, J. L. Giuliani, and A. Fruchtman, Local measurements of the spatial magnetic field distribution in a z-pinch plasma during and near stagnation using polarization spectroscopy, Phys. Plasmas **27**, 022705 (2020).
[28] V. V. Ivanov, A. A. Anderson, D. Papp, A. L. Astanovitskiy, V. Nalajala, and O. Dmitriev, Study of magnetic fields and current in the z pinch at stagnation, Phys. Plasmas **22**, 092710 (2015).
[29] V. Munzar, D. Klir, J. Cikhardt, J. Kravarik, P. Kubes, J. Malir, J. Novotny, K. Rezac, A. V. Shishlov, V. A. Kokshenev, R. K. Cherdizov, and N. A. Ratakhin, Mapping of azimuthal b-fields in z-pinch plasmas using z-pinch-driven ion deflectometry, Phys. Plasmas **28**, 062702 (2021).
[30] T. Chang, A. Fisher, and A. Van Drie, X-ray results from a modified nozzle and double gas puff z pinch, J. Appl. Phys. **69**, 3447 (1991).
[31] A. L. Velikovich, F. L. Cochran, J. Davis, and Y. K. Chong, Stabilized radiative z-pinch loads with tailored density profiles, Phys. Plasmas **5**, 3377 (1998).
[32] R. P. Golingo, U. Shumlak, and D. J. D. Hartog, Note: Zeeman splitting measurements in a high-temperature plasma., Rev. Sci. Instrum. **81**, 126104 (2010).
[33] S. V. Lebedev, F. N. Beg, S. N. Bland, J. P. Chittenden, A. E. Dangor, and M. G. Haines, Snowplow-like behavior in the implosion phase of wire array z pinches, Phys. Plasmas **9**, 2293 (2002).
[34] S. V. Lebedev, D. J. Ampleford, S. N. Bland, S. C. Bott, J. P. Chittenden, J. Goyer, C. Jennings, M. G. Haines, G. N. Hall, D. A. Hammer, J. B. A. Palmer, S. A. Pikuz, T. A. Shelkovenko, and T. Christoudias, Physics of wire array z-pinch implosions: experiments at imperial college, Plasma Phys. Controlled Fusion **47**, A91 (2005).
[35] E. M. Waisman, M. E. Cuneo, W. A. Stygar, R. W. Lemke, K. W. Struve, and T. C. Wagoner, Wire array implosion characteristics from determination of load inductance on the z pulsed-power accelerator, Phys. Plasmas **11**, 2009 (2004).
[36] M. E. Cuneo *et al.*, Characteristics and scaling of tungsten-wire-array z-pinch implosion dynamics at 20 ma, Phys. Rev. E **71**, 046406 (2005).
[37] G. N. Hall, S. A. Pikuz, T. A. Shelkovenko, S. N. Bland, S. V. Lebedev, D. J. Ampleford, J. B. A. Palmer, S. C. Bott, J. Rapley, J. P. Chittenden, and J. P. Apruzese, Structure of stagnated plasma in aluminum wire array z pinches, Phys. Plasmas **13**, 082701 (2006).
[38] G. C. Burdiak, S. V. Lebedev, G. N. Hall, A. J. Harvey-Thompson, F. Suzuki-Vidal, G. F. Swadling, E. Khoory, L. Pickworth, S. N. Bland, P. de Grouchy, and J. Skidmore, Determination of the inductance of imploding wire array z-pinches using measurements of load voltage, Phys. Plasmas **20**, 032705 (2013).
[39] C. Stollberg, Investigation of a small-scale self-compressing plasma column, Ph.D. thesis, Weizmann Institute of Science, 2019.
[40] E. Stambulchik and Y. Maron, A study of ion-dynamics and correlation effects for spectral line broadening in plasma: K-shell lines, J. Quant. Spectrosc. Radiat. Transfer **99**, 730 (2006).
[41] E. Stambulchik and Y. Maron, Stark effect of high-n hydrogen-like transitions: Quasi-contiguous approximation, J. Phys. B **41**, 095703 (2008).
[42] L. Gregorian, E. Kroupp, G. Davara, A. Starobinets, V. I. Fisher, V. A. Bernshtam, Y. V. Ralchenko, Y. Maron, A. Fisher, and D. H. H. Hoffmann, Electron-temperature and energy-flow history in an imploding plasma, Phys. Rev. E **71**, 056402 (2005).
[43] L. Gregorian, E. Kroupp, G. Davara, V. I. Fisher, A. Starobinets, V. A. Bernshtam, A. Fisher, and Y. Maron, Electron density and ionization dynamics in an imploding z-pinch plasma, Phys. Plasmas **12**, 092704 (2005).
[44] Y. V. Ralchenko and Y. Maron, Accelerated recombination due to resonant deexcitation of metastable states, J. Quant. Spectrosc. Radiat. Transfer **71**, 609 (2001).
[45] N. Konjević, A. Lesage, J. R. Fuhr, and W. L. Wiese, Experimental stark widths and shifts for spectral lines of neutral and ionized atoms (a critical review of selected data for the period 1989 through 2000), J. Phys. Chem. Ref. Data **31**, 819 (2002).
[46] I. E. Ochs, C. Stollberg, E. Kroupp, Y. Maron, A. Fruchtman, E. J. Kolmes, M. E. Mlodik, and N. J. Fisch, Current channel evolution in ideal z pinch for general velocity profiles, Phys. Plasmas **26**, 122706 (2019).
[47] M. G. Haines, The inverse skin effect, Proc. Phys. Soc. **74**, 576 (1959).
[48] M. A. Lieberman and A. J. Lichtenberg, *Principles of Plasma Discharges and Materials Processing* (John Wiley & Sons, New York, 2005).
[49] E. M. Waisman, M. E. Cuneo, R. W. Lemke, D. B. Sinars, and W. A. Stygar, Lower bounds for the kinetic energy and resistance of wire array z pinches on the z pulsed-power accelerator, Phys. Plasmas **15**, 042702 (2008).
[50] R. E. Peterkin, M. H. Frese, and C. R. Sovinec, Transport of magnetic flux in an arbitrary coordinate ale code, J. Comput. Phys. **140**, 148 (1998).
[51] T. J. Awe *et al.*, Observations of Modified Three-Dimensional Instability Structure for Imploding z-Pinch Liners that are Premagnetized with an Axial Field, Phys. Rev. Lett. **111**, 235005 (2013).
[52] J. L. Giuliani, J. W. Thornhill, E. Kroupp, D. Osin, Y. Maron, A. Dasgupta, J. P. Apruzese, A. L. Velikovich, Y. K. Chong, A. Starobinets, V. Fisher, Y. Zarnitsky, V. Bernshtam, A. Fisher, T. A. Mehlhorn, and C. Deeney, Effective versus ion thermal temperatures in the weizmann ne z-pinch: Modeling and stagnation physics, Phys. Plasmas **21**, 031209 (2014).
[53] K. N. Mitrofanov, V. V. Aleksandrov, E. V. Grabovski, A. V. Branitsky, A. N. Gritsuk, I. N. Frolov, and Y. N. Laukhin, Stability of compression of the inner array plasma in nested arrays, Plasma Phys. Rep. **43** (2017).

[54] J. I. Rozo, D. Utz, S. Vargas Domínguez, A. Veronig, and T. Van Doorsselaere, Photospheric plasma and magnetic field dynamics during the formation of solar ar 11190, Astron. Astrophys. **622**, A168 (2019).

[55] T. R. Jarboe, T. E. Benedett, C. J. Everson, C. J. Hansen, A. C. Hossack, K. D. Morgan, B. A. Nelson, J. B. O'Bryan, J. M. Penna, and D. A. Sutherland, The nature and source of solar magnetic phenomena, Phys. Plasmas **26**, 092902 (2019).